Physics Results From the National Spherical Torus Experiment

S.M. Kaye[1], M.G. Bell[1], R.E. Bell[1], J. Bialek[2] T. Bigelow[3], M. Bitter[1], P. Bonoli[4]

D. Darrow[1], P. Efthimion[1], J. Ferron[5], E. Fredrickson[1], D. Gates[1], L. Grisham[1], J. Hosea[1],

D. Johnson[1], R. Kaita[1], S. Kubota[6] H. Kugel[1], B. LeBlanc[1], R. Maingi[3],

J. Manickam[1], T.K. Mau[7] R.J. Maqueda[8], E. Mazzucato[1], J. Menard[1], D. Mueller[1],

B. Nelson[9], N. Nishino[10] M. Ono[1], F. Paoletti[2] S. Paul[1], Y-K.M. Peng[3], C.K. Phillips[1]

R. Raman[9], P. Ryan[3], S.A. Sabbagh[2], M. Schaffer[5], C.H. Skinner[1] D. Stutman[11],

D. Swain[3], E. Synakowski[1], Y. Takase[12] J. Wilgen[3], J.R. Wilson[1], W. Zhu[2], S. Zweben[1],

A. Bers[4], M. Carter[3], B. Deng[13], C. Domier[13], E. Doyle[6], M. Finkenthal[11], K. Hill[1], T. Jarboe[9],

S. Jardin[1], H. Ji[1], L. Lao[5], K.C. Lee[15], N. Luhmann[13], R. Majeski[1], H. Park[1],

T. Peebles[6], R.I. Pinsker[5], G. Porter[14], A. Ram[4], M. Rensink[14], T. Rognlien[14],

D. Stotler[1], B. Stratton[1], G. Taylor[1], W. Wampler[15], G.A. Wurden[8], X.Q. Xu[14],

L. Zeng[6] and the NSTX Team

[1]Princeton Plasma Physics Laboratory, Princeton University, Princeton, N.J. 08543

[2]Dept. of Applied Physics, Columbia Univ., NYC, N.Y.10027

[3]Oak Ridge National Laboratory, Oak Ridge, Tenn. 37830

[4]MIT, Cambridge, Mass. 02139

[5]General Atomics, San Diego, Cal., 92186

[6]UCLA, L.A., Cal.

[7]UCSD, San Diego, Cal.

[8]Los Alamos National Laboratory, Los Alamos, N.M. 87545

[9]Univ. of Washington, Seattle, Wash. 98105

[10]Hiroshima Univ., Hiroshima, Japan

[11]Johns Hopkins University, Baltimore, Md.

[12]Univ. of Tokyo, Tokyo, Japan

[13]UC Davis, Davis, California

[14]Lawrence Livermore National Laboratory, Livermore, Cal.

[15]Sandia National Laboratory, Sante Fe, N.M.

Abstract

The mission of the National Spherical Torus Experiment (NSTX) is to extend the understanding of toroidal physics to low aspect ratio (R/a$\simeq$ 1.25) in low collisionality regimes. NSTX is designed to operate with up to 6 MW of High Harmonic Fast Wave (HHFW) heating and current drive, 5 MW of Neutral Beam Injection (NBI), and Co-Axial Helicity Injection (CHI) for non-inductive startup. Initial experiments focused on establishing conditions that will allow NSTX to achieve its aims of simultaneous high-β_t and high-bootstrap current fraction, and to develop methods for non-inductive operation, which will be necessary for Spherical Torus power plants. Ohmic discharges with plasma currents up to 1 MA, stored energies up to 55 kJ, $\beta_t \sim$10%, and a range of shapes and configurations were produced. Density limits in deuterium and helium reached 80% and 120% of the Greenwald limit respectively. Significant electron heating was observed with up to 2.3 MW of HHFW. Up to 270 kA of toroidal current for up to 200 msec was produced noninductively using CHI. Initial NBI experiments were carried out with up to two beam sources (3.2 MW). Plasmas with stored energies of up to 140 kJ and β_t=21% were produced.

I. Introduction

The mission of NSTX is to extend the understanding of toroidal physics to low aspect ratio in collisionless, high-β regimes, and to demonstrate non-inductive current generation and sustainment in these regimes. These are necessary ingredients for a Spherical Torus (ST) power plant. In order to validate the ST concept, it is necessary to attain MHD stable high-β_t plasmas, with β_t in excess of 40%, at the low toroidal magnetic fields characteristic of STs.[1,2] Herein, β_t is defined as $2\mu_0 < p > / B_0^2$ where B_0 is the vacuum toroidal field at the geometric radius. Good confinement is needed in order to attain high-β_t, and both enhanced MHD stability and reduced microturbulence are potential benefits of an increased region of good field line curvature in the ST configuration. Because of the narrow center column in STs, the inductive flux will be severely limited, and thus noninductive startup and current sustainment, including high bootstrap current fraction, would be an essential feature of ST reactors. Lastly, the compact nature of the ST means that power fluxes to the plasma facing components may be quite severe, and, therefore, effective power handling strategies must be developed. The National Spherical Torus Experiment (NSTX) was developed in the wake of both encouraging theoretical predictions for performance,[3–6] and experimental achievements in low aspect ratio devices.[7,8] A more complete discussion of these key physics issues, and how the physics basis of NSTX was developed in order to address these issues, can be found in Kaye et al[9] and Peng.[10]

NSTX discharges that are MHD stable and have adequate confinement will have to be developed in order to achieve high-β. Furthermore, the non-inductive current drive tools, many of these ST specific, must also be developed to demonstrate this essential feature of operation. Necessary first steps in achieving these goals are to explore operational space, and to understand and overcome the physics and technical limitations encountered in order to map out the best route to high performance.

Recent results from NSTX can be found in References.[11–15]

II. Device Description

The NSTX device was designed with the capabilities necessary to study the key physics issues in STs. The nominal device and plasma parameters are: R_0/a=0.85 m/0.67 m=1.26, I_p=1 MA, B_T=0.3 T with capability up to 0.6 T, $\kappa \leq 2.2$, $\delta \leq 0.5$ for q_{95} ~10 to 15, allowing access to the high β_t, high bootstrap current regime,[5] and eventually plasma pulse lengths of up to 5 sec, to allow the study of current profile relaxed plasmas. Auxiliary heating and current drive tools are 5 MW of 80 keV D^0 Neutral Beam Injection (NBI), 6 MW of High Harmonic Fast Wave (HHFW) heating and current drive at 30 MHz, and Co-Axial Helicity Injection (CHI) with up to 50 kA of CHI injector current and 1 kV injector voltage. Both the NBI and HHFW are designed to operate for up to 5 sec, and calculations indicate that approximately 200 kA of plasma current can be driven by co-NBI (mostly on-axis) while up to 400 kA of off-axis current can be driven by HHFW in fully developed plasmas.[9] CHI will be developed to substitute for inductive flux during plasma startup and as a possible means of driving current near the plasma periphery during the fully developed plasma phase.[16]

A cross-section of the device is shown in Fig. 1, and a complete device description can by found in Neumeyer et al.[17] The center stack is the most critical element in the NSTX design, and it consists of a steel tension tube over which is wound the OH solenoid, and on which are mounted magnetic diagnostics and thermocouples. The OH and PF coils systems can provide approximately 1 W of flux. The center stack casing is an inconel tube, which also serves as the vacuum vessel inner wall, on which are mounted alternating rows of ATJ and CFC graphite tiles. The center stack is cooled inertially, and it is demountable. Also seen in the figure are the 1/2" thick copper passive conducting plates on the outboard side to aid in the vertical and low-n stability of the plasma. ATJ graphite tiles line the passive and divertor plates. The outer vacuum vessel and center stack casing are connected through bellows that allow for relative movement between the two due to thermal effects, and through ceramic insulators that provide electrical insulation between the outboard divertor plate and

center stack casing, which are the primary electrodes for CHI operation.

The HHFW launcher consists of 12 poloidal conducting straps and six transmitters with flexible phasing that subtends approximately 90° in the toroidal direction. Each antenna strap is protected by a molybdenum Faraday shield as well as by boron nitride shields on the top and bottom, and between each launcher. Plasma breakdown is aided greatly by an 18 GHz, 10 to 15 kW Electron Cyclotron preionization system. A bakeout system that will heat the internal plasma facing components (plates, centerstack, and tiles) up to 350° C, and the outer vacuum vessel to 150° C, will be used to aid in conditioning.

The plasma control system uses the Plasma Control Software (PCS) originally written at General Atomics for use on DIII-D.[18] Actual control algorithms are NSTX specific.[19] The system runs on a SKYBOLT-I real-time computer, with communication between the machine operator and real-time computer through a SPARC-10 host computer. The real-time computer is presently being upgraded to a SKYBOLT-II with G4 processors, which will allow implementation of the real-time EFIT control algorithm, also developed at General Atomics.[20]

III. Results

A. Ohmic Operational Space and Performance

The NSTX device began operation in Feb. 1999, and after several days of operation with open loop plasma control, discharges with 300 kA of plasma current were achieved. After this short commissioning run, the device was opened to install most of the remaining internal hardware components. Ohmic operations restarted in Sept. 1999, and during the next four months, experiments to explore OH flux consumption, operational limits and equilibrium configurations, along with preliminary High Harmonic Fast Wave (HHFW) and Co-axial Helicity Injection (CHI) studies, were carried out. During this time, the device achieved transient currents of up to 1 MA, the design value of the machine. HHFW and

CHI studies were carried out also during this period. Following a six month down period to install and commission additional device components and diagnostics, including the installation of the neutral beam, operation resumed in July 2000 with closed loop position control. NBI commenced in mid-Sept. 2000.

One of the major impediments to achieving high performance operation during the Autumn 1999-Winter 2000 experimental campaign was the MHD activity believed to be related to a high impurity content in the plasmas,[21] in part due to exposed copper of the passive plates. In order to reduce these impurities, the bare copper was covered with graphite tiles during the most recent opening, and a variety of wall cleaning techniques was subsequently employed.[22] These included center stack bakeout via resistive heating, glow discharge cleaning (GDC) in deuterium and helium, helium conditioning plasma discharges, and most recently, several boronizations by introducing trimethylboron gas during helium GDC. Reference deuterium discharges following boronization showed a factor of over 10 reduction in oxygen, a factor of 33% decrease in carbon, and a reduction in copper to undetectable levels (Fig. 2a). The loop voltage in post-boronization discharges generally decreased by 20 to 30%, conserving inductive flux and improving the ability to achieve high current discharges, as shown in Fig. 2b. Also seen is the reduction in radiated power in the post-boronized plasmas. The Ejima coefficient, a measure of the resistive flux consumption, decreased to values of $\sim$0.3 with average current ramp rates of 5 MA/sec,[12] allowing plasma currents of up to 1.07 MA to be attained. Higher ramp rates led to reduced flux consumption due to the reduction in plasma inductance, but were prone to MHD activity.

A portion of the initial operational period was devoted to establishing NSTX operational space. Equilibrium development studies led to the production of plasmas in Inner Wall Limited, Double Null and Lower Single Null Divertor configurations. A poloidal flux surface plot, as computed by the EFIT magnetics reconstruction code,[13] for a high triangularity (δ=0.42) double null divertor discharge is shown in Fig. 3a. Elongations from 1.2 to 2.5 and triangularities from 0.2 to 0.5 (0.6 transiently) were achieved (see Fig. 3b).

Boronization was also crucial to extending the achievable density in both deuterium and helium. Fig. 4a shows the achieved line-averaged electron density measured by Thomson scattering as a function of the Greenwald parameter, $n_{eGW} = I_p/\pi a^{2}$[23] for both species. As can be seen, the pre-boronized plasmas attained densities up to only $0.6n_{eGW}$ for either species. After boronization, the achieved densities were considerably higher, with deuterium plasmas reaching $0.8n_{eGW}$ (4×10^{19} m^{-3}) and helium reaching $1.2n_{eGW}$ (5.5×10^{19} m^{-3}). One major difference between the two species was the amount of Carbon III light, which was much greater in deuterium most likely due to chemical sputtering of the graphite tiles. For both species, in both pre- and post-boronized plasmas, the radiated power increased with increasing density, but was still low, typically $\leq 40\%$ of the ohmic power at the time of maximum density (Fig. 4b). The radiated power was measured by a 16-channel tangential bolometer array located at the midplane, and the volume integrated power was calculated assuming that the radiated power is constant on along a flux surface. The only MHD activity typically observed at the time of the density limit in the highest density cases was sawteeth. However, sawteeth were also observed at lower densities, indicating, along with the relatively low radiated power fractions, that fueling limitations probably set the maximum density.

A low-q limit was encountered at $q_{cyl} = 2.5a^2 B_T(1+\kappa^2)/RI_p = 2$ by ramping down the toroidal field at constant plasma current. The limit was manifest by a low toroidal mode number (m=2) kink instability that started to grow when the q=2 surface, as determined by EFIT, reached to within 10 cm of the plasma edge. The mode was apparent in visible light images of the plasma.

Confinement times in both deuterium and helium discharges exhibit trends that are similar to those at conventional aspect ratio, and these are shown in Figs. 5a and b. The confinement times are calculated in EFIT reconstructions, whose stored energies have uncertainties of $\pm 20\%$. For low to moderate densities ($\leq 4 \times 10^{19}$ m^{-3}, corresponding to $0.8n_{eGW}$ at $I_p = 0.7$ MA), the confinement time in both species increases approximately

linearly with line-averaged density to a value of 45 msec. This effect is seen most clearly in Figs. 5b, where the variation in plasma current (600 to 900 kA) and other parameters have been normalized out. At $n_e/n_{eGW} \leq 0.8$, the maximum confinement time is approximately $1.4\tau_{ITER89P}$,[24] while $\tau_E/\tau_{ITER89P}$=0.8 to 1.0 at the higher densities. The confinement time drops to values of about 20 msec at the highest density (5.5×10^{19} m^{-3}), corresponding to $1.2n_{eGW}$. For the ITER89P scaling used in Fig. 5b, the mass scaling parameter was taken to be M_{eff}/Z_{ion}, which is 2 for either species. The maximum ohmic confinement times are comparable to values given by ELMy H-mode scalings.

The dominant mode affecting plasma performance at present in both ohmic and auxiliary heated plasmas is a large m=1/n=1 mode leading to sawteeth that result in a reduction in core pressure and a saturation and rollover in stored energy (Fig 6a). The reason for the large effect of the sawteeth is the large radius of the q=1 surface, which is shown in Fig 6b. The q-profile shown in this figure, which is determined from an EFIT reconstruction, exhibits an extended region of low shear where $q \leq 1$. The q=1 surface is close to 2/3 of the way out towards the edge of the plasma, and these positions agree quite well with the sawtooth inversion layer as determined from the soft X-ray array.

Under certain circumstances, however, stable discharges could be produced. One of the MHD instabilities that has been observed during all phases of NSTX discharges is the internal or global Reconnection Events (RE). This event is characterized by Mirnov oscillations, spikes in $I_p,\ D_\alpha$, and Carbon-III, and modification of the plasma internal inductance and elongation. The REs depend strongly on vessel conditioning. As discharge conditions improved with the wall conditioning techniques mentioned earlier, the frequency of REs decreased, and with proper gas programming it was possible to avoid REs altogether, during all phases of the discharge. Fig. 7a shows the time evolution of a 0.5 MA, MHD-free discharge lasting for 0.5 sec. During the course of this discharge, q_0, as computed by EFIT, decreases to near and slightly below one. A comparison of this MHD quiescent discharge with the MHD active one shown in Fig. 6a reveals distinct differences in l_i and $r(q = 1)$,

the radius of the q=1 surface, as is shown in Fig. 7b. At the time of the onset of instability in the MHD active discharge, l_i (top panel) is lower than in the MHD quiescent one, indicating a broader current profile, consistent with what was shown in Fig. 6b. In addition, the q=1 radius (bottom panel) appears in the plasma sooner, and, consistent with the lower l_i, is at an approximately 10 cm larger radius than that in the MHD quiescent discharge. The MHD quiescent discharge has a lower plasma current than the MHD active one, which will certainly affect the q_0 and the q-profile, but this comparison n3evertheless indicates the importance of controlling the current profile to avoid the deleterious effect of MHD activity. Furthermore, it indicates that the higher q_0, and more peaked current profiles (i.e., smaller q=1 radius) lead to more stable plasmas.

Finally, it should be mentioned that halo currents arising from plasma disruptions have been measured on NSTX and have been found to be benign. The fastest current decay rates on NSTX were found to be associated with Vertical Displacement Events due to loss of vertical control, and these decay rates reached -400 MA/sec. Halo currents measured on the center stack and passive plate support legs indicate peak magnitudes of 20 to 30 kA, corresponding to 3 to 5% of the maximum current.

B. Electron Heating with High Harmonic Fast Waves

As shown in the previous section, tools are clearly needed to modify the q-profile in NSTX into one that is more favorable to MHD stability. Further, it is desirable to have a mechanism to heat the electrons to both reduce the resistive flux consumption further, and to allow for higher levels of bootstrap current. Because of the high dielectric constant in ST plasmas ($\epsilon = \omega_{pe}^2/\Omega_{ce}^2$=10 to 100) as compared to that in conventional aspect ratio tokamaks ($\epsilon \leq$1), electron heating and current drive mechanisms in the Electron Cyclotron and Lower Hybrid range of frequencies cannot be used because of lack of wave accessibility.

Fast waves at high harmonics (5 to 20) of the majority ion cyclotron frequency, however, can provide electron heating and current drive through electron Landau damping of the

waves in the high-β, high dielectric constant plasmas.[25] The High Harmonic Fast Wave (HHFW) system on NSTX has the real-time capability of varying the launched $k_{||}$ from 14 to 4 m^{-1} in order to heat the plasma efficiently from a low temperature (300 eV) target to a high temperature ($\geq$ keV) condition. A gap of approximately 5 cm between the antenna and plasma edge was found to be optimal for coupling the RF power to the plasma.

Fig. 8a shows the time evolution of two helium discharges, one with and one without RF, at comparable plasma currents (700 kA) and densities ($n_{e0} \simeq 3.5 \times 10^{19}$ m^{-3}). The discharge with RF had an injected power of nearly 2.3 MW with a launched $k_{||}$ of 14 m^{-1}. As is seen in the figure, the central electron temperature (900 eV) is approximately 400 eV greater in the RF discharge than in the one without RF. The electron temperature and density profiles as measured by the Thomson scattering system are shown in Fig. 8b, revealing an increase in the temperature with RF across the entire profile, consistent with off-axis deposition at these temperatures. As can be seen in the lower panel of Fig. 8b, the electron density was approximately the same for discharges. The electron heating, which has resulted in central electron temperatures greater than 1 keV, has so far been observed only at the slowest wave phase velocity ($k_{||} = 14$ m^{-1}).

As is further shown in Fig. 8b for this discharge, the stored energy reached 60 kJ (β_t=10%), and the loop voltage was 1 V in comparison to 1.35 V without RF. The RF plasma exhibited higher levels of radiation than that without RF, due to an increase in edge carbon radiation, but the radiated power levels were still low ($P_{rad} \sim 0.15$ MW $\sim P_{RF}/15$). A large m=1/n=1 mode is seen to grow in the soft X-rays and Mirnov coils, eventually leading to an MHD event that terminated the heating and dumped the RF power to the wall. This 1/1 activity is seen in discharges without RF as well.

The RF heating was modeled using the 1-D METS95[26] and 2-D TORIC[27] codes. The METS code is particularly suited to determining the strength and midplane mapping of the power damped on the ions and electrons in one transit of the waves across the plasma. Results of the METS calculation are shown in Fig. 9. Calculations were performed for

both the target plasma (T_{e0}=400 eV) and the RF-heated plasma (T_{e0}=900 eV) conditions. As can be seen from the power absorption profiles in the figure, the single pass absorption is nearly 100% for both phases of the discharge, with only a fraction of the power during the RF phase being absorbed by minority hydrogen ions (assumed to be 2% of the total ion density). The oscillations in the absorption profiles come from waves reflected at a high-field side cut-off. The METS modeling indicates that the absorption moves farther off-axis in the hotter plasmas, serving to broaden the electron temperature profiles, consistent with the observations of heating across the entire profile as shown in Fig. 8b. These 1-D results are confirmed by initial results from the CURRAY ray tracing[28] and 2-D TORIC codes.

C. Non-Inductive Current Generation Using Co-Axial Helicity Injection

Successful generation of toroidal current by CHI relies on first generating poloidal current on open field lines. This is accomplished on NSTX by biasing the center stack with respect to the outer vacuum vessel, both of which are insulated from each other by ceramic breaks at the top and bottom of the vessel. Poloidal field coils are used to set up a favorable poloidal field pattern in the lower divertor region. The electron cyclotron pre-ionization system generates a plasma in the injector region, allowing poloidal current to flow on open field lines between the inner and outer lower divertor plates. A sufficient poloidal current flowing in the presence of a toroidal field can overcome the field line tension and cause the plasma to move up into the main chamber due to the $J_{pol} \times B_{tor}$ force, with the current establishing a toroidal component in order to remain force free. CHI on NSTX is a significant extension of experiments on HIT-I, -II[16] and HIST[29] with its much greater volume and pulse lengths (30$\times$ for both).

A sequence of plasma images of a CHI generated plasma is shown in Fig. 10. The images are taken by the LANL fast camera which has a fish-eye view of the entire plasma

chamber (the center stack is in the middle of the image). The plasma is generated by using a typical pre-fill pressure of 0.2 to 2 Pa. The sequence clearly shows the plasma originating in the lower divertor region (t=16 msec) and extending into the main chamber at later times (t=18, 20 msec). The injector current generating this discharge was 7 kA, resulting in a toroidal current of 20 kA.

Fig. 11 shows time traces from a CHI discharge in which approximately 20 kA of injector current produced an OH-free discharge with a total pulse length of 200 msec and a 50 msec flattop toroidal current over 200 kA. The ”flux utilization efficiency” for this discharge, which is essentially the fraction of injector flux that is transferred to the confinement region to set up the toroidal current there, reaches one from 140 to approximately 200 msec. To date, transient toroidal currents of up to 270 kA have been driven by CHI in NSTX.

A major issue for these CHI discharges is whether the poloidal flux surfaces remain open or are closed. At present, this is still under investigation by both data analysis and modeling. One of the signatures of the magnetic reconnection process that has led to flux closure in other devices is the presence of global low-n mode activity seen on Mirnov coils.[16] While activity of this nature has been seen in some of the CHI discharges, it is absent or weak in others. The issue of flux closure and the processes responsible for it will be an area of investigation in future CHI experiments.

Ultimately, CHI plans for NSTX include both adding OH flux to an already established CHI discharge, or adding CHI to drive edge current in an inductively produced plasma. In either case, the vessel pressure must be compatible for both CHI and inductive operation. CHI plasmas have been produced in NSTX with main chamber neutral pressures down to 200 mPa, while ohmic discharges have been produced with pressures reaching up to 130 mPa. Thus, the level of neutral pressure in both types of discharges are comparable.

D. Initial NBI Discharge Characterization

The ability to achieve high-β_t plasmas in NSTX requires not only adequate confinement, but also an effective means to heat the plasma. HHFW is a new approach to heating the plasma, as described above. Since Neutral Beam Injection (NBI) has been consistently successful as a heating source in toroidal fusion devices, this method of heating method is also being used on NSTX. The installed beam line consists of three 80 keV sources that can deliver up to 5 MW of D^0 power to the plasma for up to 5 sec. The three sources, A, B and C have tangency radii of 70, 60, and 50 cm respectively. Only sources B and C (for a total of 3.2 MW) were available for the initial NBI experiments, which began in mid-September.

High performance plasmas were produced after only a few weeks of NBI experiments. These experiments were carried out at plasma currents of 0.5 to 1.0 MA and toroidal fields of 0.3 to 0.4 T. Fig. 12a shows the time evolution of a one source (P_{inj}=1.6 MW) discharge at 1.0 MA and 0.4 T. The 1 MA current flattop duration for this discharge was approximately 185 msec, which is a duration consistent with that predicted for NBI discharges.[9] The plasma stored energy reached a value of 122 kJ, as computed by the EFIT magnetic reconstruction code. The value of stored energy from this calculation has an uncertainty of $\pm$20%, although preliminary measurements from the diamagnetic loop show agreement with the EFIT values. Attempts are presently underway to verify these values based on kinetic profiles. The stored energy in this discharge started to decrease at t=270 msec, and this energy loss is associated with the onset of sawteeth as q_0 dropped to values below one, similar to the behavior of OH discharges. The Thomson scattering electron temperature and density profiles for this discharge near the time of peaked stored energy are shown in Fig. 12b. The central electron temperature was just over 1 keV (1.1 keV was achieved in other discharges) with the central density reaching 5×10^{19} m^{-3}. The slight dip in the core density at this time may be due to the presence of m=1/n=1 activity. Other discharges at this toroidal field exhibited an interesting time evolution, in which, after the beams were on for approximately 140 msec and the electron temperature reached a steady state, there was

a sudden jump in the electron temperature across the central half of the plasma, reminiscent of the creation of core transport barriers.[30] This evolution will be investigated further with respect to the q-profile and/or rotational shear.

Plasma discharges with β_t=21% (β_n=4.1, 115 kJ of stored energy at $q_\psi = 7.5$) using the two beam sources (P_{inj}=2.8 MW) were achieved. Also, impressive discharges with β_t=19.7% (β_n=3.9) using only one beam source (P_{inj}=1.3 MW) were produced. Fig. 13a shows an example of the time evolution of one of these discharges. The plasma current was raised to 1 MA and was held constant for a duration of over 100 mec. The beam source was turned on at 90 msec, and β_t increased continuously to its maximum value of 19.7%, corresponding to 106 kJ. The energy confinement time at the time of maximum β_t, uncorrected for shine-thru and prompt orbit loss, was 40 msec, which is approximately 35% above the value given by the ITER89P L-mode scaling, and about 10% above ELMy H-mode scaling. Poloidal flux contours for this discharge are shown in Fig. 13b. The increase in β_t was abruptly terminated by growth of MHD activity that occurred as q_0 dropped below one. These results again point to the need to develop MHD suppression methods to allow the achievement of even higher β_t.

The first series of experiments also focused on understanding the beam heating efficiency in light of the large particle orbits (gyroradius $\sim$ banana width) due to the low toroidal field in NSTX and STs in general. Fig. 14a shows the plasma stored energy as a function of beam source and plasma current during NBI. The stored energy exhibits a nearly linear dependence with plasma current, as expected from both the dependence of thermal confinement from conventional scalings, and a higher prompt ion loss at lower current as indicated by model calculations. Thus, this dependence on plasma current may be due to two different effects, the thermal confinement and the available number of fast ions for heating. The results also show that the stored energy increment is lower for Source C than for Source B, in general, and this confirms the modeling calculations which indicate increasing prompt loss with decreasing tangency radii (particles born well on the

inside which then are lost to the outside). It is seen that the heating efficiency is poor for both sources at 500 kA, as evidenced by the low stored energy increment relative to the ohmic value at this current. Interestingly, the stored energy increments for Sources B and C combined are comparable to the sum of the increments for each source separately at each current, indicating little or no degradation of incremental confinement with power.

The increase in stored energy with increasing toroidal field for one and two source discharges is shown in Fig 14b. Experiments with toroidal fields up to 0.4 T were performed, with plasma stored energies reaching 140 kJ.

The energy confinement time, normalized to the values determined from various scaling expressions, is plotted as a function of toroidal field for two source discharges (P_{inj}=2.55 to 3.2 MW in Fig. 15. The expressions used to normalize the confinement time are ITER89P L-mode and three recent ELMy H-mode scalings.[31] These experimental confinement times are computed using the full injected power, without corrections for shine-thru or prompt orbit loss, and thus are underestimates of the actual confinement time. The normalized confinement times increase with increasing toroidal field, although it is difficult to say whether this trend is due to better beam confinement (not expected to be a big effect for this limited variation in toroidal field), reduced MHD activity at higher B_T, or whther it is the global manifestation of reduced local transport. This notwithstanding, the confinement times are significantly above those given by L-mode scaling (up to 1.55$\times$), as well as above H-mode values at the higher B_T (up to 1.35$\times$). These initial confinement results are quite encouraging for NSTX to be able to attain the level of confinement necessary for achieving high-β_t.

IV. Summary and Future Plans

The initial operating period of NSTX focused on developing the basic operational and physics understanding that is necessary for advancing the ST concept. Among the most

important are establishing operating regimes that will enable the achievement of good confinement and suppressed MHD, leading to high-β_t and high bootstrap fraction, and the non-inductive generation and sustainment of current. Wall conditioning techniques, most importantly boronization and helium GDC, along with careful gas programming, resulted in stable discharges allowing operation at high density and ohmic confinement times enhanced over L-mode values. Initial NBI experiments resulted in discharges with up to 140 kJ of stored energy, and $\beta_t$values of up to 21%, along with T_{e0} values up to 1.1 keV and long ($\leq$200 msec) current flattop durations at 1 MA. Initial confinement estimates indicate good confinement, with enhancements of up to 1.6 over L-mode and 1.35 over ELMy H-mode scalings. Both OH and auxiliary heated discharges, however, exhibited large sawteeth, caused by an extended region of low shear where q$\leq$1, which caused a significant loss of plasma stored energy. This points to the importance of developing techniques to control the current profile. One of these techniques, potentially, is HHFW, which, for the initial heating experiments, led to significant electron heating, serving to reduce the inductive flux consumption. Toroidal current was produced successfully by completely non-inductive means, with up to 270 kA of toroidal current generated by CHI.

Future research will concentrate on developing the tools and physics understanding further. The NBI and HHFW systems will be brought to their full capability in 2001. HHFW will be used not only to heat the electrons further to reduce the inductive flux consumption further and also allow for a high bootstrap current at these higher electron temperatures, but to drive current in the outer regions of the plasma as well in an attempt to maintain q_0 above one in order to prevent MHD activity. CHI will attempt to produce 500 kA target plasmas. High temperature bake and between-shots GDC will be used to further condition the walls. Confinement studies will turn towards extending the understanding of both global and local transport properties in this new regime. Finally, β_t-limit studies in first stability regime plasmas (β_t=25%, $f_{bs} \simeq 0.4$) will assess the need for active wall mode

stabilization for optimizing the performance of NSTX.

ACKNOWLEDGEMENTS

This work was supported by US Department of Energy Contract DE-AC02-76CH03073 at the Princeton Plasma Physics Laboratory, DE-FG02-89ER53297 at Columbia University, DE-AC05-96OR22464 at Oak Ridge National Laboratory, DE-FG06-90ER54095 at the University of Washington, W-7405-ENG-36 at the Los Alamos National Laboratory, DE-AC03-99ER54463 at General Atomics, DE-AC04-94AL85000 at Sandia National Laboratory, and DE-FG02-99ER-54521 at MIT.

References

[1] R. Buttery and et al., Steady state spherical tokamaks and future applications, in *Plasma Phys. Cont. Nuclear Fusion Research*, volume 2, page 633, Vienna, Austria, 1995, IAEA, (Proc. 15th Int. Conf. Seville, 1994).

[2] M. Peng and et al., Physics progress towards compact tokamak reactors with normal conducting toroidal field coils, in *Plasma Phys. Cont. Nuclear Fusion Research*, volume 2, page 643, Vienna, Austria, 1995, IAEA, (Proc. 15th Int. Conf. Seville, 1994).

[3] M. Peng and D. Strickler, Nucl. Fusion **26**, 769 (1986).

[4] G. Rewoldt and et al., Phys. Plasmas **3**, 1 (1996).

[5] J. Menard and et al., Nucl. Fusion **37**, 595 (1997).

[6] R. Stambaugh and et al., The Spherical Torus approach to magnetic fusion development, in *Fusion Energy 1996*, volume 2, page 395, Vienna, Austria, 1997, IAEA, (Proc. 16th Int. Conf. Montreal, 1996).

[7] D. Gates and et al., Phys. Plasmas **5**, 1775 (1998).

[8] A. Sykes, R. Akers, L. Appel, and et al., Phys. Rev. Lett. **84**, 495 (2000).

[9] S. Kaye, M. Ono, Y.-K. Peng, and et al., Fusion Technology **36**, 16 (1999).

[10] Y.-K. Peng, Phys. Plasmas **7**, 1681 (2000).

[11] M. Ono and et al., Overview of the initial NSTX experimental results, Proceedings of the 18^{th} IAEA Fusion Energy Conference, Sorrento, Italy, 2000.

[12] J. Menard and et al., Flux consumption optimization and the achievement of 1 MA discharges on NSTX, Proceedings of the 18^{th} IAEA Fusion Energy Conference, Sorrento, Italy, 2000.

[13]S. Sabbagh and et al., Equilibrium properties of Spherical Torus plasmas in NSTX, Proceedings of the 18^{th} IAEA Fusion Energy Conference, Sorrento, Italy, 2000.

[14]J. Wilson and et al., High harmonic fast wave heating on NSTX, Proceedings of the 18^{th} IAEA Fusion Energy Conference, Sorrento, Italy, 2000.

[15]R. Raman and et al., Non-inductive current generation in NSTX using Co-axial helicity injection, Proceedings of the 18^{th} IAEA Fusion Energy Conference, Sorrento, Italy, 2000.

[16]T. Jarboe and et al., Recent results of the Helicity Injected Tokamak experiment, in *Fusion Energy 1996*, volume 2, page 243, Vienna, Austria, 1997, IAEA, (Proc. 16th Int. Conf. Montreal, 1996).

[17]C. Neumeyer and et al., Engineering design of the National Spherical Torus Experiment NSTX, to be published in Fusion Engineering and Design, 2000.

[18]J. Ferron and et al., in *Proceedings of the 16^{th} IEEE/NPSS Symposium on Fusion Energy, Champaign, Ill. 1996*, volume 2, page 870, IEEE, (IEEE Inc., Piscataway, 1996), 1996.

[19]D. Gates, in *Proceedings of the 11^{th} IEEE/NPSS Real-Time Conference, Sante Fe, 1999*, page 278, IEEE, (IEEE Inc., Piscataway, 1999), 1999.

[20]J. Ferron and et al., Nucl. Fusion **38**, 1055 (1998).

[21]R. Maingi and et al., Initial wall conditioning and impurity control techniques in NSTX, Proceedings of the 27^{th} EPS Conference on Controlled Fusion and Plasma Physics, Budapest, Hungary, 2000.

[22]H. Kugel and et al., Overview of impurity control and wall conditioning in NSTX, to be published in J. Nucl. Mat., 2000.

[23]M. Greenwald and et al., Nucl. Fusion **28**, 2199 (1988).

[24]P. Yushmanov and et al., Nucl. Fusion **30**, 1999 (1990).

[25]M. Ono, Phys. Plasmas **2**, 4075 (1995).

[26]D. Smithe and et al., Proceedings of Conference on RF Power in Plasmas, AIP, N.Y., p. 267, 1997.

[27]M. Brambilla, Plasma Phys. Controlled Fusion **1**, 41 (1999).

[28]T. Mau, S. Chiu, and R. Harvey, Proceedings of the EPS Topical Conference on RF Heating and Current Drive of Fusion Devices, Brussels, p. 181, 1992.

[29]M. Nagata and et al., in *Fusion Energy 1998*, Vienna, Austria, 1998, IAEA, (Proc. 17th Int. Conf. Yokahama, 1998).

[30]M. Bell and et al., Plasma Phys. Control. Fusion **41** (1999).

[31]I. Team, Nucl. Fusion **39**, 2175 (1999).

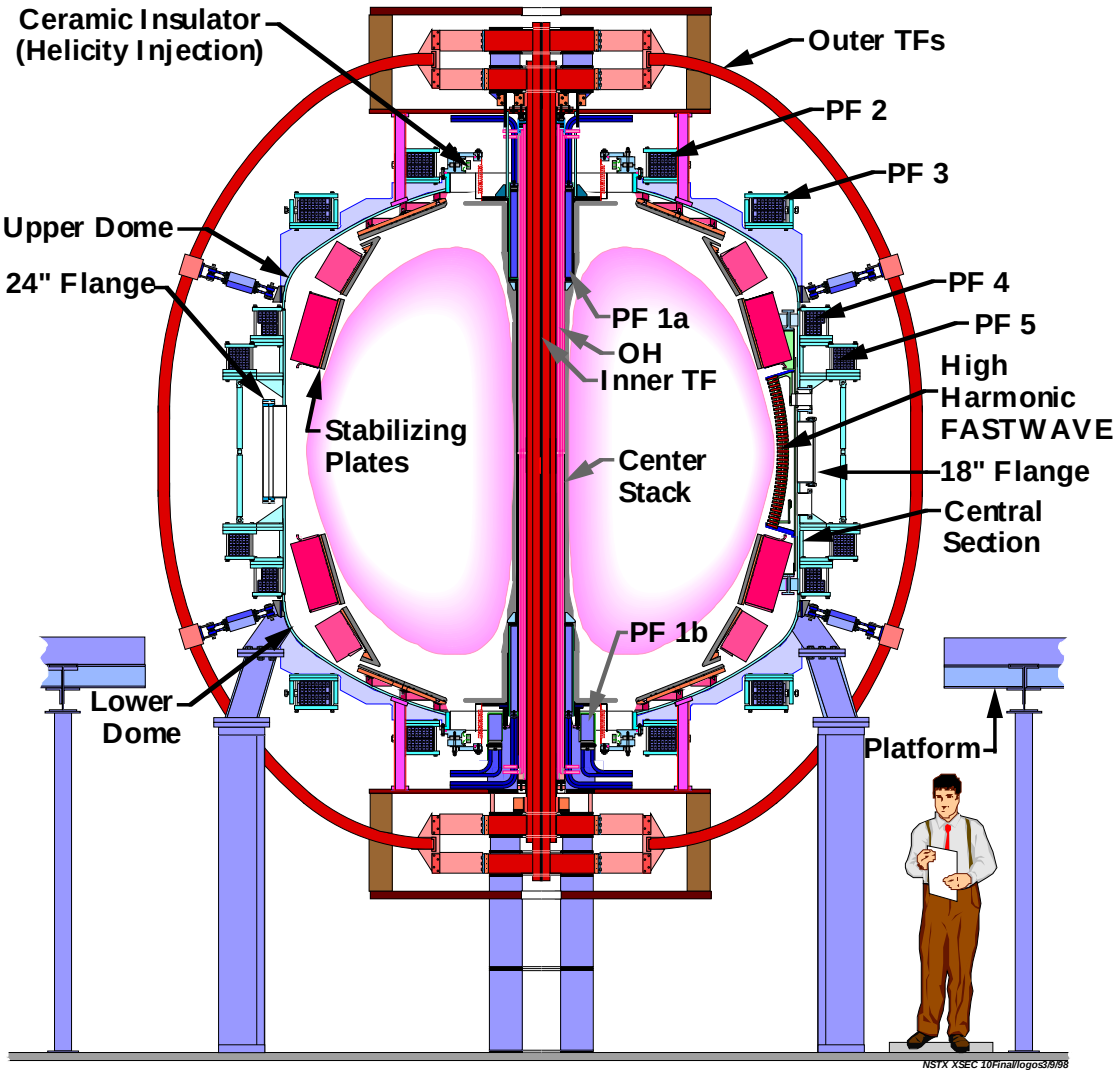

Figure 1: NSTX Cross-Section

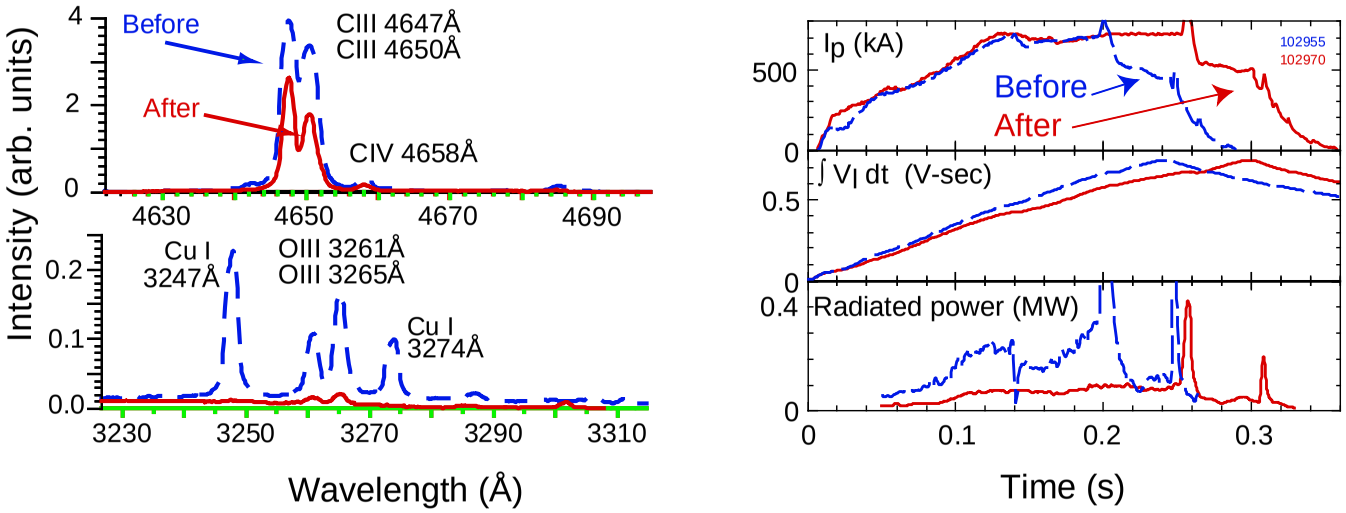

Figure 2: (a) Impurity line spectra from pre- and post-boronized plasmas. (b) Time evolution of pre- and post-boronized D2 ohmic plasma showing the reduction in inductive flux consumption and radiation in the post-boronized case.

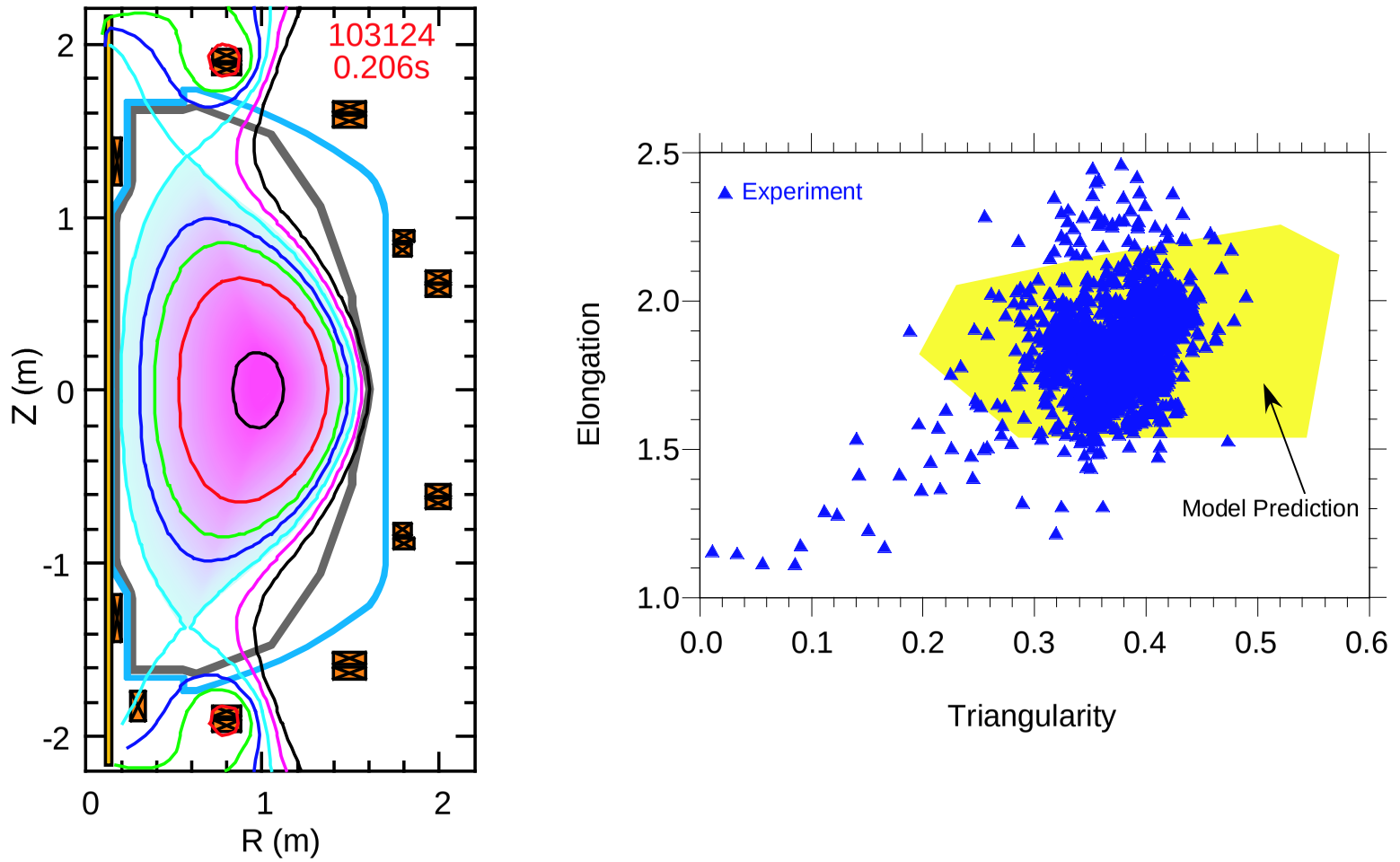

Figure 3: (a) Flux surface plot for a high triagularity ($\delta = 0.43$) double-null divertor discharge. (b) Achieved elongation vs triangularity.

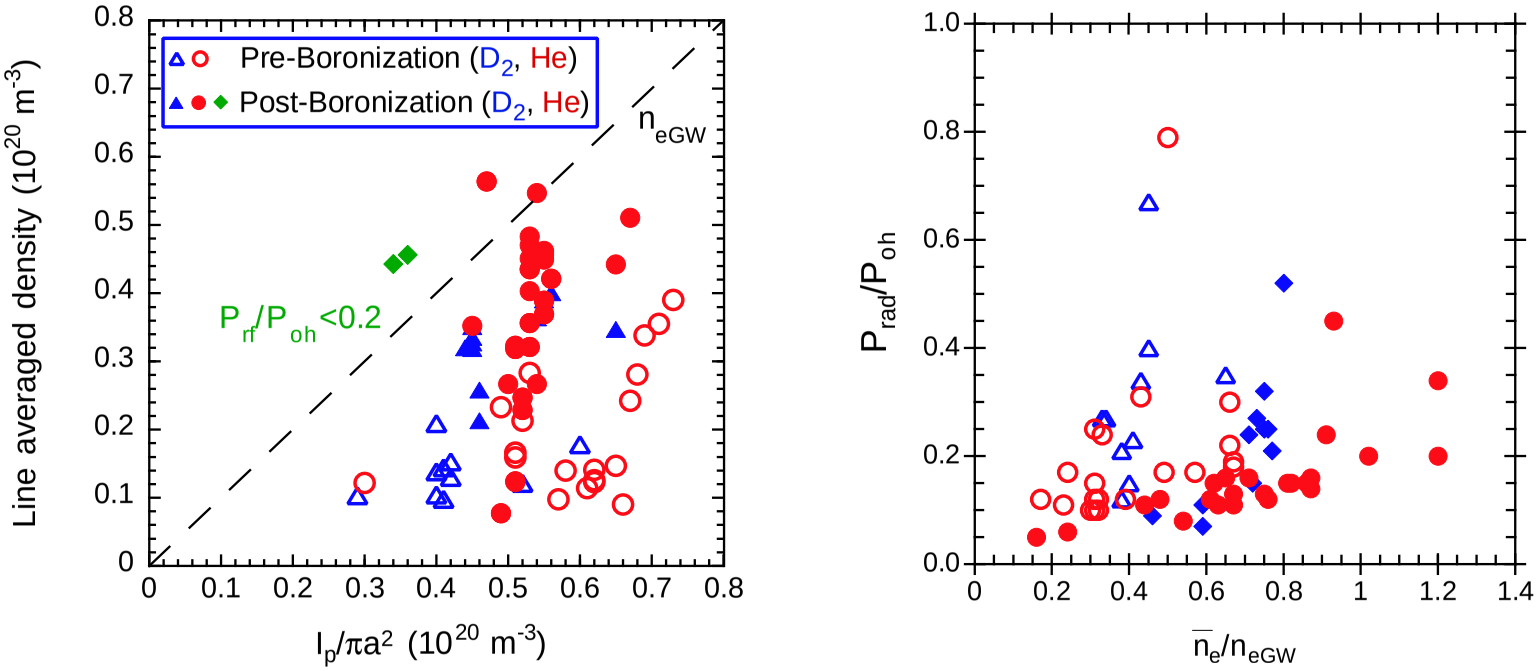

Figure 4: (a) Line averaged density vs Greenwald parameter for ohmic discharges. (b) Radiated power fraction as a function of Greenwald fraction.

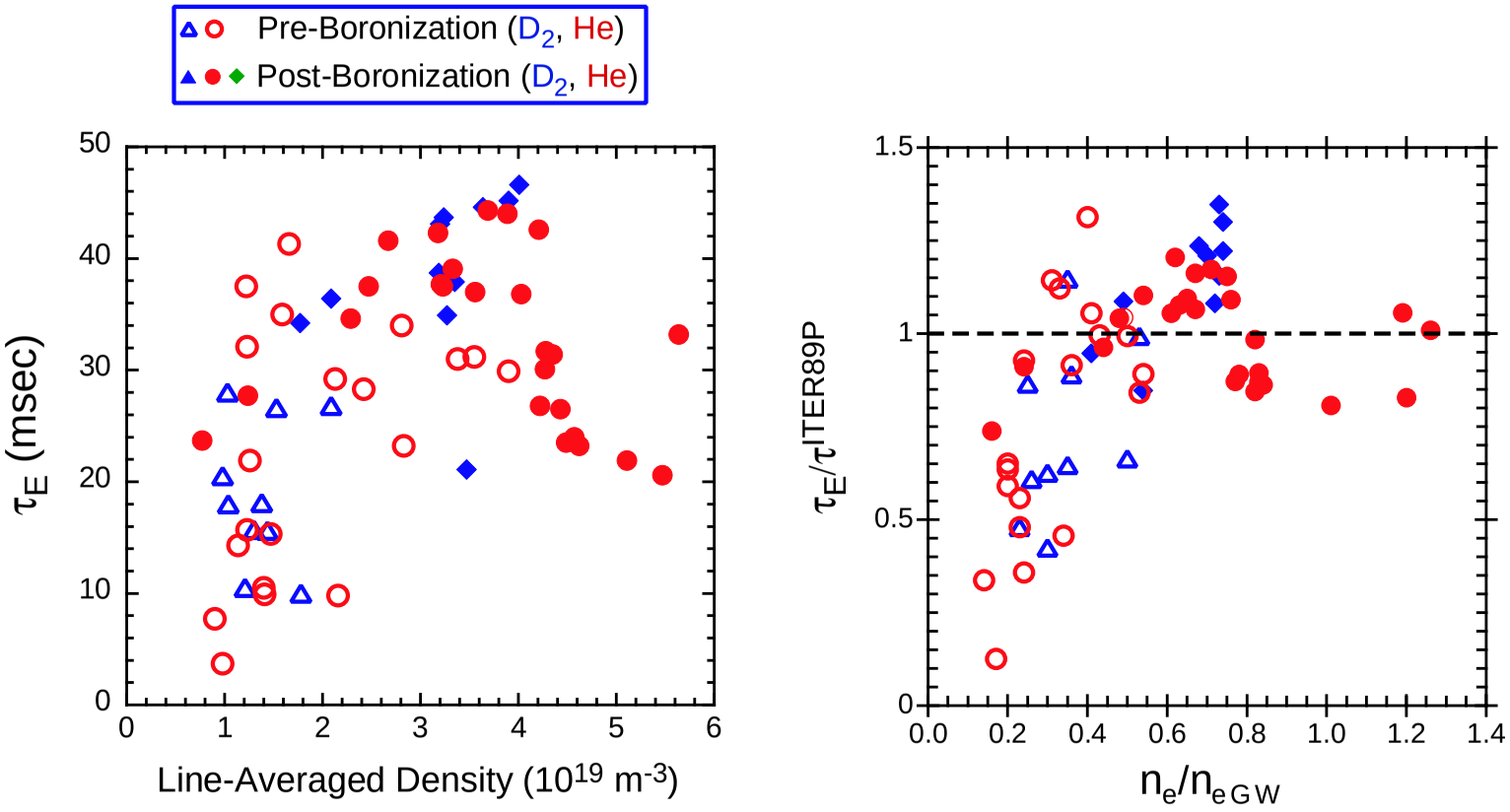

Figure 5: (a) Ohmic confinement time as a function of line-averaged density. (b) Ohmic confinement time normalized to the ITE89P scaling value as a function of fraction of Greenwald density.

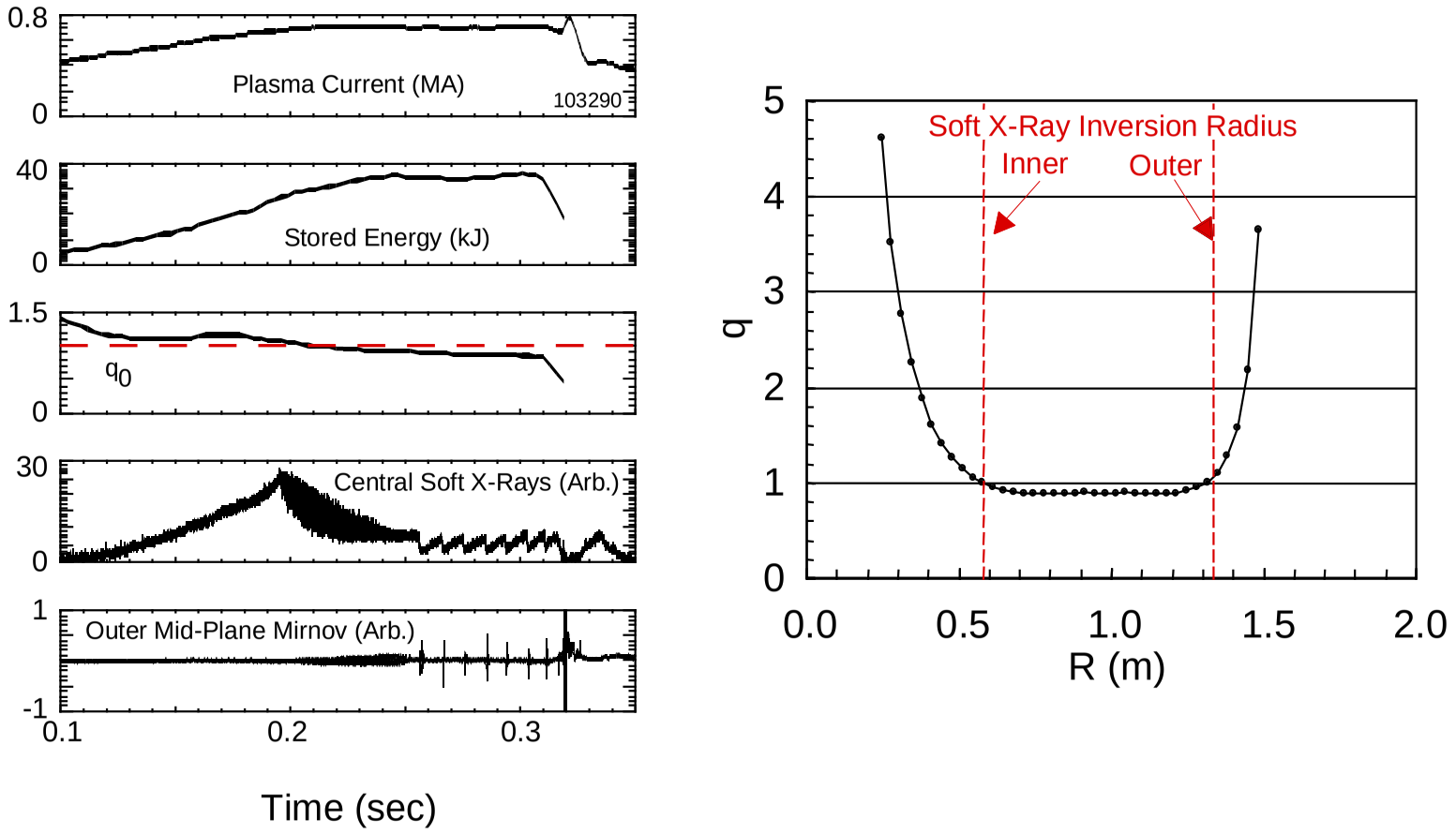

Figure 6: (a) Ohmic discharge exhibiting m=1/n=1 mode and sawteeth. (b) q-profile as determined from EFIT. The arrows indicate the location of the sawtooth inversion radius from the Soft X-ray array.

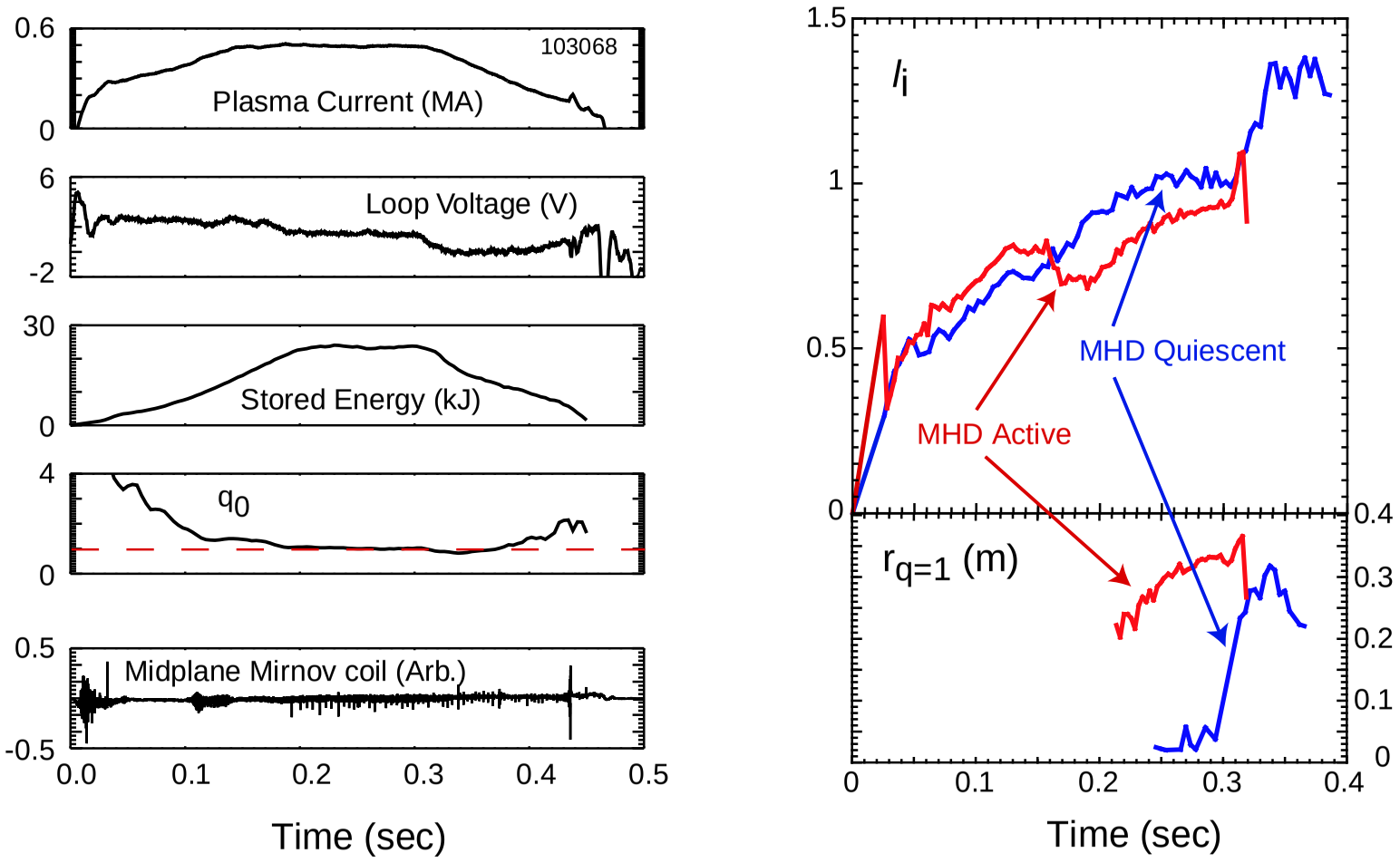

Figure 7: (a) MHD-free Ohmic discharge. (b) l_i (top panel) and the postion of the q=1 radius (bottom panel) as determined by EFIT.

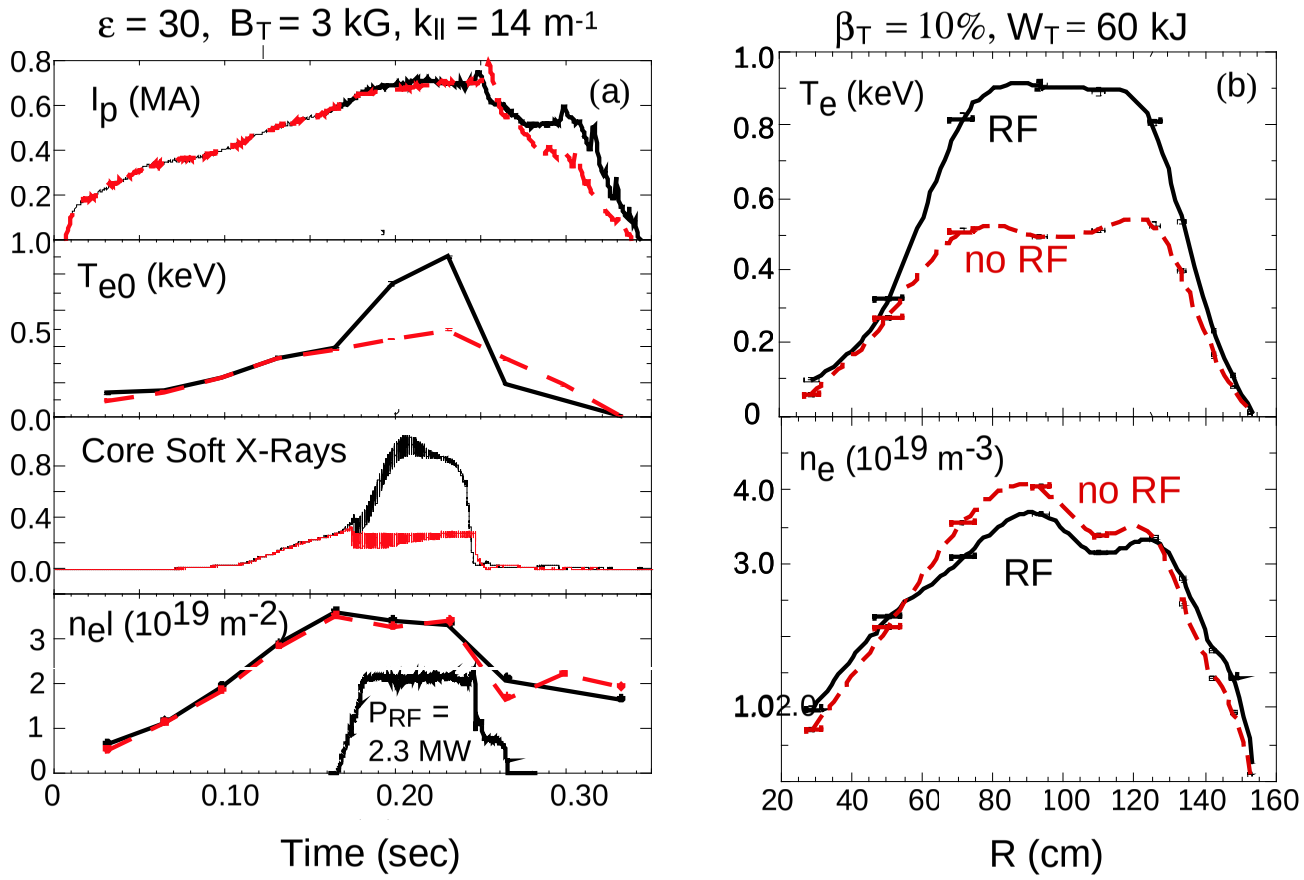

Figure 8: (a) Time evolution of discharge parameters with and without RF heating. (b) Electron temperature and density profiles from Thomson Scattering with and without RF heating.

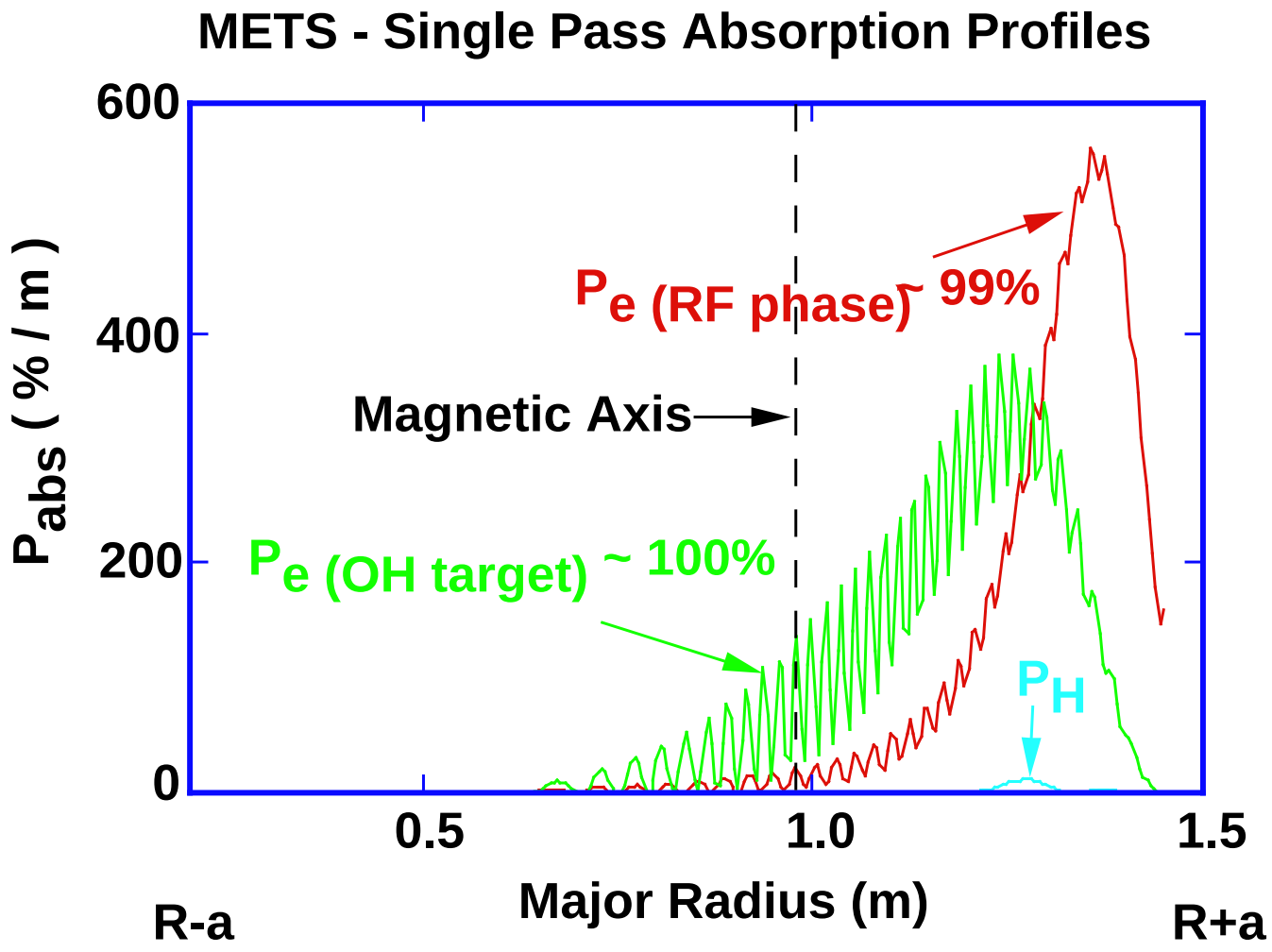

Figure 9: METS 1-D modeling of RF absorption in an RF-heated plasma. Shown are power absorption profiles for both the OH target and RF phases of the discharge.

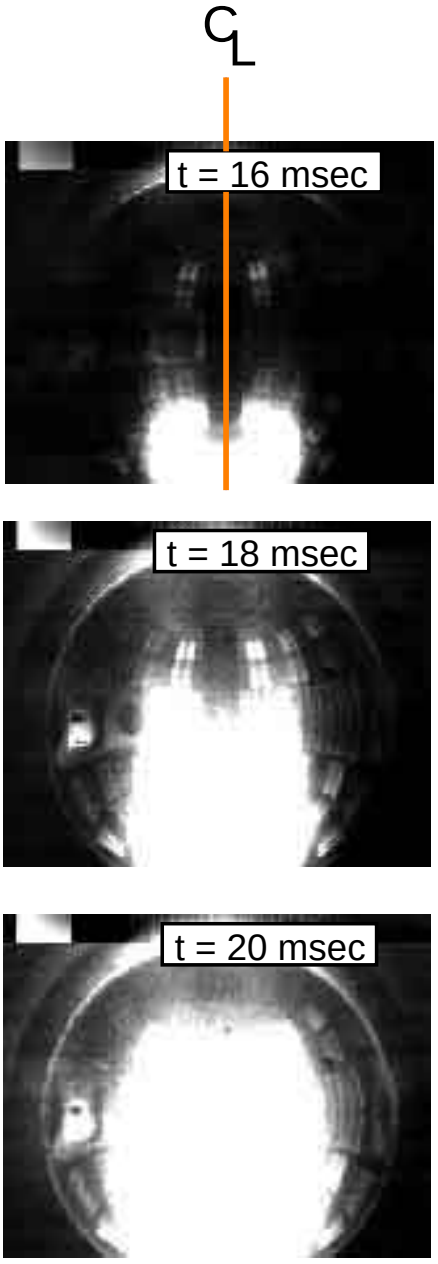

Figure 10: Fast camera images across the entire vessel of CHI plasma startup showing injection from the lower part of the vessel, near the electrodes, proceeding to fill the vessel.

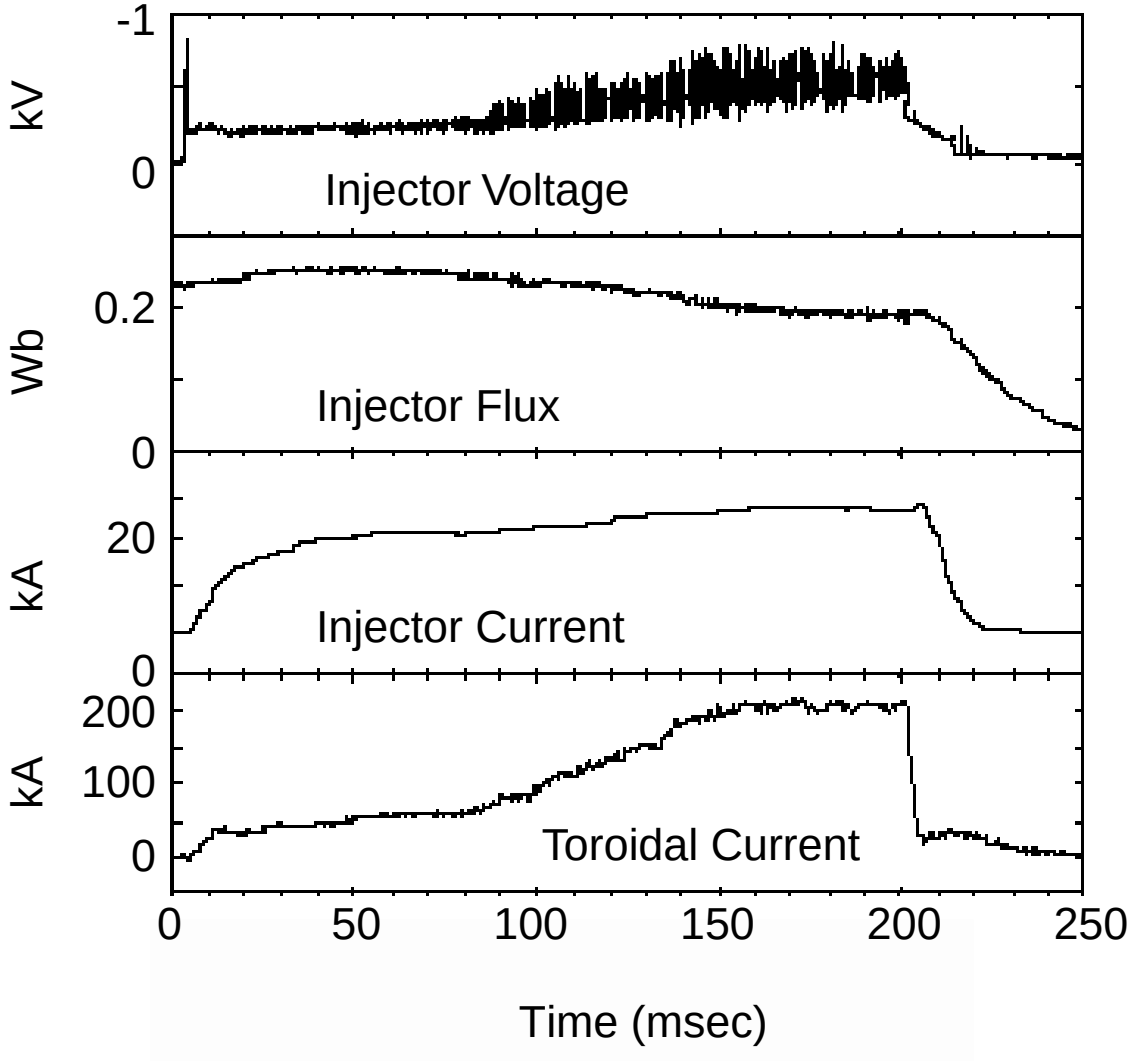

Figure 11: Time evolution of a CHI plasma discharge reaching over 200 kA.

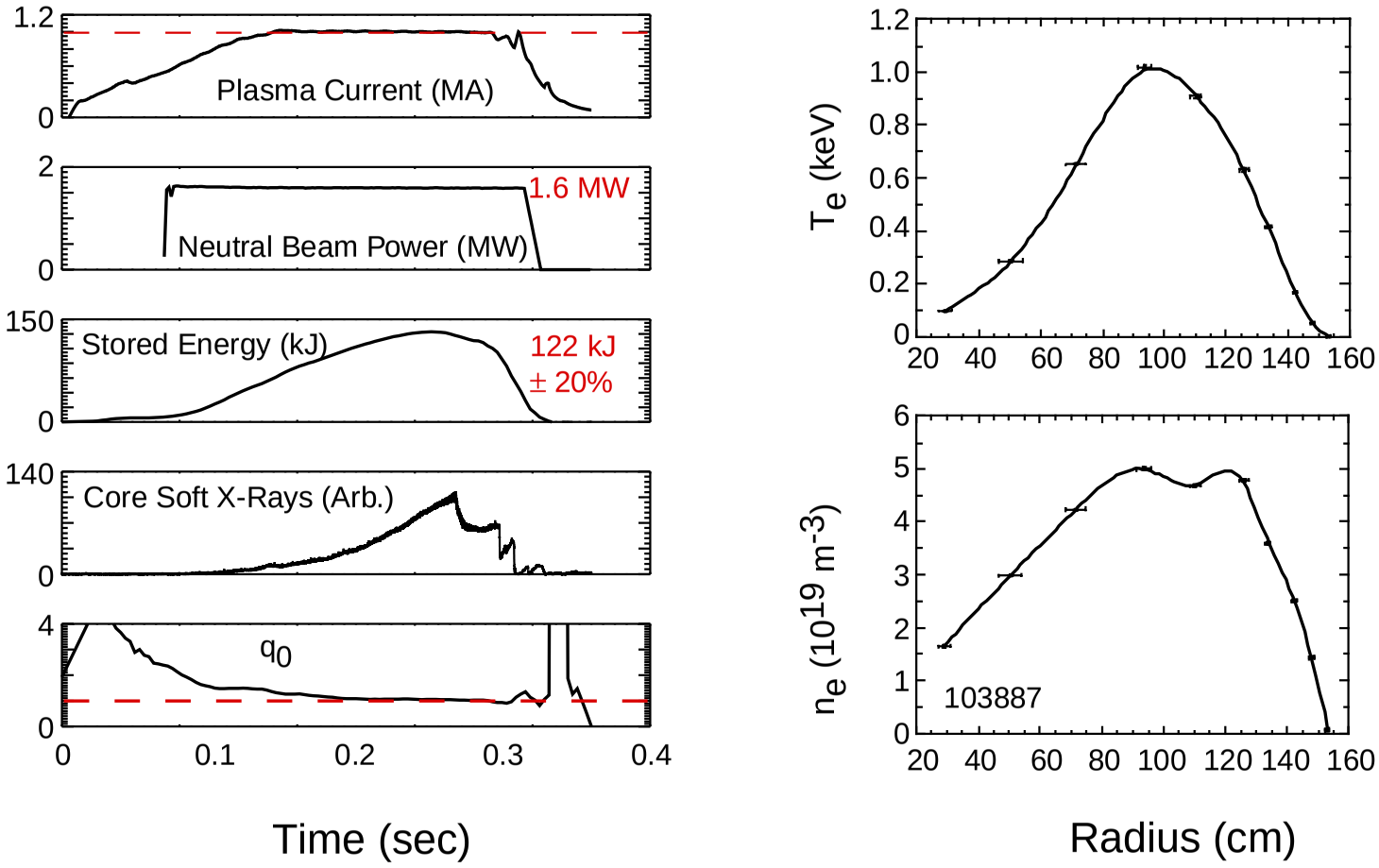

Figure 12: (a) Time history of a one source (P_{inj}=1.6 MW) discharge with a 1 MA current flattop duration of 185 msec. (b) Electron temperature and density profiles from Thomson scattering at the time of maximum stored energy for this discharge.

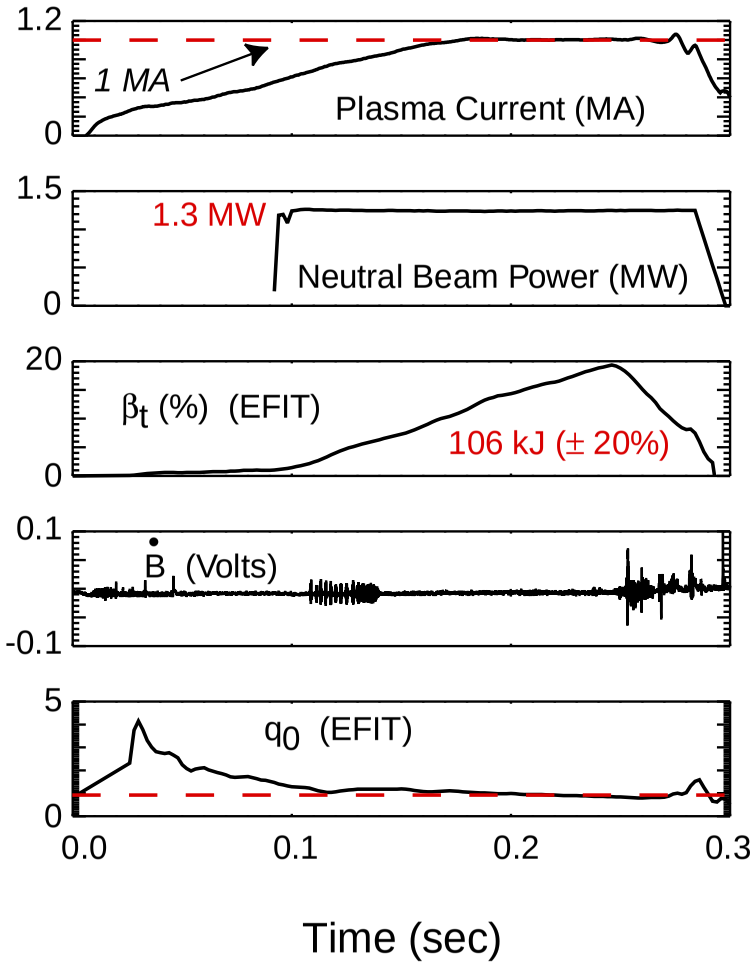

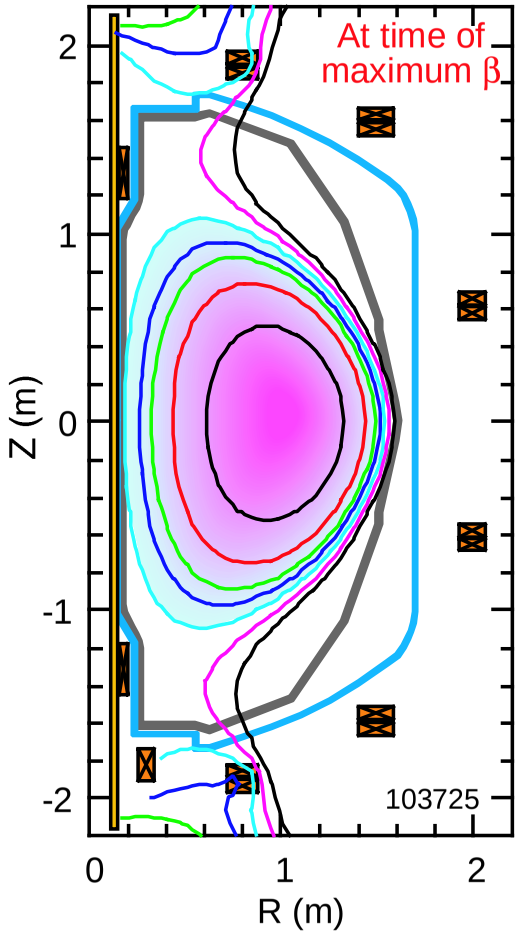

Figure 13: (a) Time history of the one source ($P_{inj} = 1.3$ MW, β_t=19.7% discharge. (b) Poloidal flux contours at the time of maximum β_t.

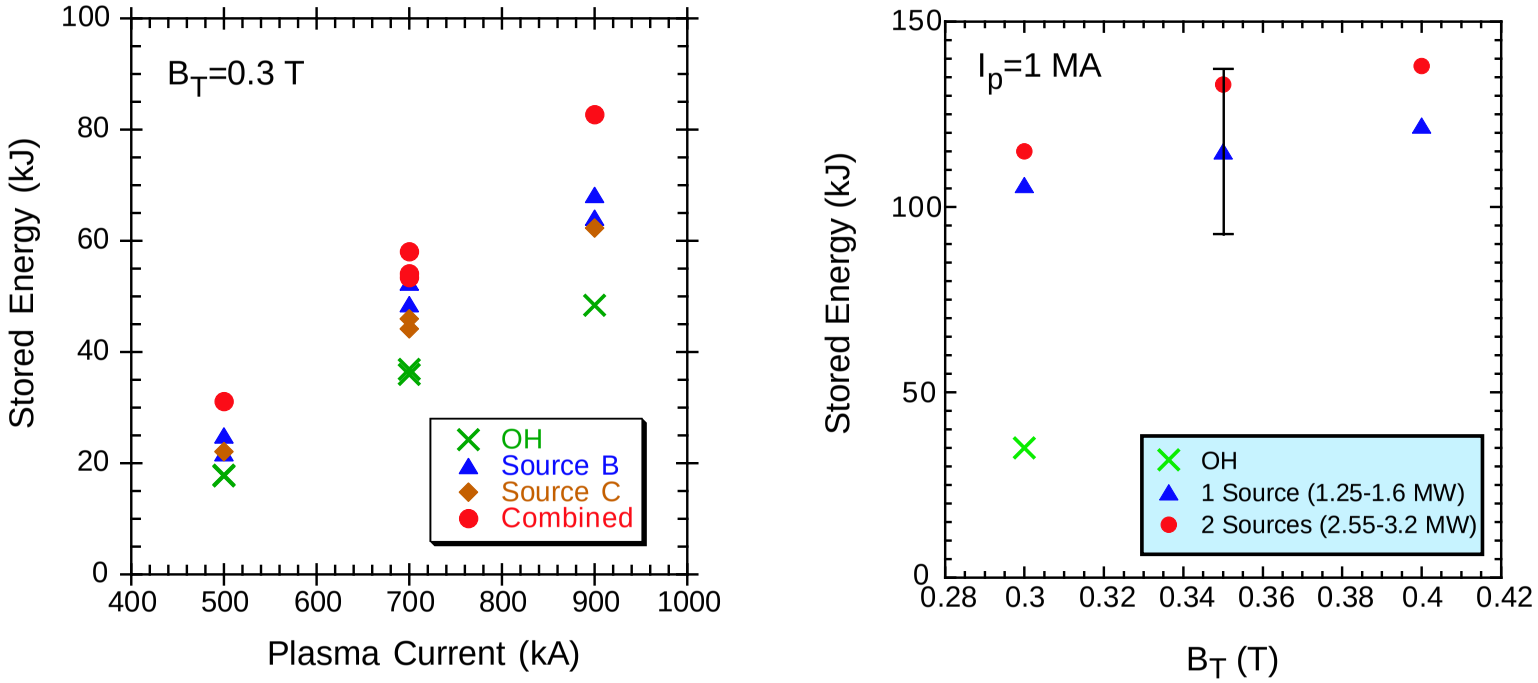

Figure 14: (a) Stored energy from EFIT as a function of plasma current and beam source for 0.3 T discharges. (b) Stored energy as function of toroidal field for 1 MA discharges. Shown is the extent of the 20% uncertainty of the EFIT determination of stored energy.

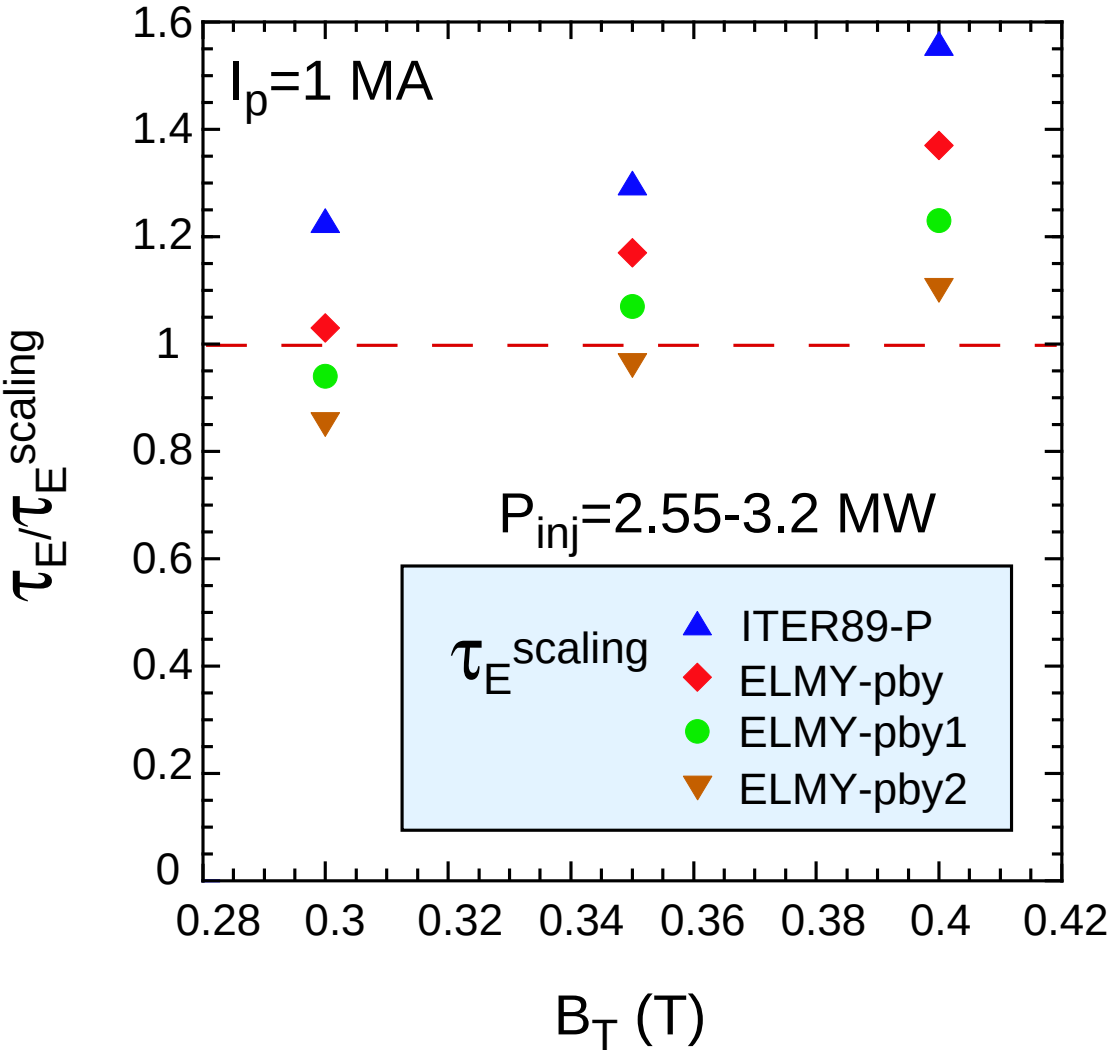

Figure 15: Confinement time for 1 MA, two source discharges normalized to four scaling values as a function of toroidal field.